Phase identification of 850-nm-thick 7%$YO_{1.5}$-93%HfO_2 films by Raman spectroscopy

Takanori Mimura[1,5], Yuma Takahashi[1], Takahisa Shiraishi[1], Masanori Kodera[1], Reijiro Shimura[1], Keisuke Ishihama[1], Kazuki Okamoto[1], Hiroki Moriwake[2], Ayako Taguchi[2], Takao Shimizu[3], Yasuhiro Fujii[4], Akitoshi Koreeda[4] and Hiroshi Funakubo[1]

[1]Materials and Chemical Technology, Tokyo Institute of Technology, Japan

[2]Nanostructures Research Laboratory, Japan Fine Ceramics Center, Japan

[3]Research Center for Functional Materials, National Institute for Materials Science, Japan

[4] Department of Physical Sciences, Ritsumeikan University, Japan

[5] Department of Chemistry, Faculty of Science, Gakushuin University, Japan

funakubo.h.aa@ m.titech.ac.jp;

Abstract

Phase identification of 850-nm-thick 7%$YO_{1.5}$-93%HfO_2 films was carried out not only by conventional X-ray diffraction (XRD) but also by analyzing both the surface and cross-sectional Raman spectra. Preparation of 7%$YO_{1.5}$-93%HfO_2 films was conducted by deposition at room temperature on Pt-coated (100)Si substrates by pulsed laser deposition and post-heat-treatment at 600–1100°C under atmospheric N_2 flow. The cross-sectional Raman spectra changed with the post-heat-treatment temperature in accordance with the crystal structure determined by XRD measurements. Moreover, surface Raman analysis revealed that the crystalline phase transformed from the tetragonal phase ($P4_2/nmc$) to the orthorhombic phase ($Pca2_1$) when an electric field was applied. These data clearly show that Raman spectroscopy is a powerful tool for detecting the constituent phase with a spatial resolution on the order of several micrometers. In addition, a good signal-to-noise ratio was obtained from the cross-sectional Raman spectrum of 850-nm-thick 7%$YO_{1.5}$-93%HfO_2 films, indicating promise for future measurements of the strain state and phase distribution along the thickness direction using this good spatial resolution.

(164 words)

1. Introduction

The ferroelectricity of HfO_2-based films was first reported in 2011.[1] Owing to good compatibility with the complementary metal oxide semiconductor (CMOS) process and good scalability, HfO_2-based ferroelectrics have become a major research field because of their nonvolatile memory applications.[2] In addition to such memory applications, their piezoelectric, optoelectric, and pyroelectric properties have also been investigated after realizing the ferroelectricity of films thicker than 1 μm.[3–5]

There are many crystal symmetry phases derived from the fluorite structure in the HfO_2-based system, and the ferroelectric phase of the HfO_2-based film is a non-centrosymmetric orthorhombic phase ($Pca2_1$), as ascertained by transmission electron microscopy (TEM).[6,7] This phase is metastable; therefore, reproducible production of this ferroelectric phase is one of the main concerns in obtaining stable ferroelectricity. Therefore, phase identification is critical to understand the ferroelectricity of these films. X-ray diffraction (XRD) is a useful characterization method for phase identification. However, because of the similarity of the ferroelectric phase ($Pca2_1$) to other phases, including the monoclinic ($P2_1/c$), tetragonal ($P4_2/nmc$), and cubic ($Fm\bar{3}m$) phases, phase identification remains ambiguous, especially for distinguishing between the tetragonal and orthorhombic phases.[8] A conventional XRD θ–2θ scan generally cannot distinguish these two phases when the lattice parameter is changed by the strain. The detection of several diffraction spots observed in the lower-symmetry orthorhombic phase, such as *110* and *211*, are the only way to distinguish between these two phases.[6,9] However, these spots are generally difficult to detect in polycrystalline films because of their weak intensities. A more complicated problem is that the polar non-centrosymmetric orthorhombic phase ($Pca2_1$) and its antipolar centrosymmetric phase (*Pbca*) are

indistinguishable by XRD measurements.[8] Although the antipolar phase has not been mentioned extensively in most reported papers, identifying this phase is important for understanding the wake-up and fatigue mechanisms that have been discussed.[10]

Raman spectroscopy is used to solve these difficulties in distinguishing the ferroelectric phase from other phases, as shown in Fig. S1.[11–13] The relatively higher spatial resolution of Raman spectroscopy compared to that of laboratory-scale XRD enables identification of the phase distribution on the substrate. In addition, Raman spectra can reveal the strain state in films by visualizing the distribution of the constituent phase and residual strain on the wafer scale.[14,15] The high spatial resolution also allows observation of the constituent phase under or after the application of an electric field, as demonstrated for ferroelectric $Pb(Zr,Ti)O_3$ films.[16] However, there are only a few studies on Raman spectroscopy of HfO^2-based ferroelectric films.

The ferroelectric orthorhombic $Pca2_1$ phase is known to be metastable and is commonly obtained in films less than 30 nm thick owing to the size effect.[5] This hinders the acquisition of sufficient Raman intensity for analysis, slowing the study of Raman spectroscopy in ferroelectric HfO_2-based films. Recently, the preparation of thicker films with a ferroelectric phase has been reported. Starschich *et al*. showed 100–390-nm-thick ZrO_2 films using chemical solution deposition (CSD).[17] Additionally we prepared 1-μm-thick Y-doped HfO_2 films using pulsed laser deposition (PLD). Previously, Yashima *et al*. reported orthorhombic phases (γ_1 and γ_2) with unknown space groups for quenched bulk Y-doped HfO_2.[18] Therefore, Y-doping is considered effective for fabricating thick films and bulk materials with a ferroelectric phase.[5] Subsequently, Xu *et al*. prepared bulk single-crystal Y-doped HfO_2 using a laser-diode-heated floating-zone technique.[19]

The Raman responses of the HfO_2 polymorphs have been calculated and are

presented in several papers.[11–13,20,21] Phase identification with the calculated Raman spectral patterns was achieved for bulk single-crystalline Y-doped HfO_2, 45-nm-thick Si-doped ZrO_2, 100-nm-thick ZrO_2, and 60-nm-thick Ta-doped HfO_2 films.[11,20,22,23] These results show the dependence of the Raman spectrum on the Y, Si, and Ta dopant concentrations. Moreover, some studies have performed Raman analysis using thick films by stacking alternating Al_2O_3 interlayers and $Hf_xZr_{1-x}O_2$ films. Schroeder *et al*. reported the concentration and annealing condition dependence of Raman spectra using $Hf_xZr_{1-x}O_2$ films.[21] Materano demonstrated the phase change in ZrO_2 films by applying an electric field using Raman spectroscopy.[20] These studies revealed that Raman spectroscopy is a useful method for identifying the crystalline phases in HfO_2-based films and bulk materials. However, knowledge of the Raman analysis of HfO_2-based films is not as deep as that for other ferroelectrics. In this study, we focused on thick Y-doped HfO_2 films. For thick films, a good Raman signal-to-noise ratio is expected to be obtained from the cross-section as well as the surface. The strain state is known to significantly change the crystal structure of HfO_2 films.[24] Therefore, the Raman spectra along the film thickness direction for a thick film can also be used to investigate the strain state and crystal phase distribution in the film.[12,15]

In this study, we systematically compare the Raman spectroscopy and XRD analysis results using 850-nm-thick $7\%YO_{1.5}$-$93\%HfO_2$ films prepared by room temperature deposition followed by heat treatment at 600–1100°C. Raman spectroscopy can clearly distinguish the ferroelectric orthorhombic phase ($Pca2_1$) from the tetragonal and antipolar orthorhombic (*Pbca*) phases, unlike XRD, revealing the dependence of the crystal phase on the heat-treatment temperature. A field-induced phase transition from tetragonal to orthorhombic $Pca2_1$ phase was observed for films heat-treated at 900°C.

These results demonstrate that Raman spectroscopy is a powerful tool for identifying crystalline phases. Moreover, the thick 7%$YO_{1.5}$-93%HfO_2 film exhibited Raman spectra with good signal-to-noise ratios from the cross-section as well as from the surface. The Raman spectra of this thick film will be useful for future investigations into the relationship between the strain and crystalline phase in the film thickness direction.

2. Experimental

Approximately 850-nm-thick 7%$YO_{1.5}$-93%HfO_2 films were prepared on (111)Pt/TiO_x/SiO_2/(001)Si substrates by a pulsed laser deposition (PLD) method using a KrF excimer laser (λ = 248 nm). The substrate temperature and atmosphere were maintained at room temperature and 10 mTorr of O_2, respectively. Laser repetition and deposition rates were 10 Hz and 40 nm/h, respectively. The films were post-heat-treated at 600–1100ºC for 10 s under N_2 flow using a rapid thermal furnace.

Macroscopic XRD was performed to determine the crystal phases (D8 DISCOVER, Bruker). The electrical properties were measured using 100-nm-thick Pt-top electrodes (φ = 50 and 100 μm) prepared by electron beam evaporation. The ferroelectricity of the films was measured at room temperature under 10 kHz using polarization–hysteresis (*P*–*E*) curves.

An Ar^+ laser (514.5 nm) with a power of 50 mW was used for the Raman experiments. The incident laser was focused on the fractured cross-section and surface of the films using an object lens (N. A. 0.70). The size of the focused laser spot was approximately 1 μm. The scattered light was collected using a backscattering geometry and single monochromator (Photon Design PDPT 640F). Spectra were obtained using a Peltier-cooled charge-coupled device detector.

3. Results and discussion

XRD analysis was performed as the first step to characterize the films heat treated at various temperatures. Figures S2 and S3 show XRD ψ–2θ scans near the {111} and {110} peaks of 7%$YO_{1.5}$-93%HfO_2 films. The {110} peaks shown in Fig. S3 reveal the existence of orthorhombic and/or monoclinic phases because these peaks do not exist in the tetragonal phase owing to the distinction rules. The classification of the orthorhombic *Pca*2_1 and *Pbca* phases is difficult by XRD measurement due to their similar diffraction patterns. Broad {111} and {110} peaks were observed at approximately ψ = 55° and 45°, respectively. This suggests that these films have a {100} surface-normal orientation, which has been reported for thick 7%$YO_{1.5}$-93%HfO_2 films owing to their self-orientation characteristics.[5]

Fig. 1(a) shows the θ–2θ XRD patterns of {111} peaks located at 2θ = 25–35° integrated along the ψ direction of the data shown in Fig. S2. The subscripts "*o*", "*t*", and "*m*" in Fig. 1 denote orthorhombic, tetragonal, and monoclinic phases, respectively. This measurement can distinguish the monoclinic phase from other higher symmetry orthorhombic or tetragonal phases because the *11-1* and {111} peaks of the monoclinic phase are located at approximately 28° and 31°, separate from the peaks of higher symmetry phases located at 2θ =~30°, as shown in Fig. 1(a). The as-deposited film consisted of a monoclinic phase, but a higher-symmetry phase was observed in the films heat treated at higher temperatures. Fig. 2(a) shows the XRD intensity ratio of $I_{(111o+101t)}/\{I_{(111o+101t)}+ I_{(111m)}+ I_{(11\text{-}1m)}\}$ obtained from Fig. 1(b). The peak intensity was estimated using peak fitting, as shown in Fig. S4(a), where $I_{(111o+101t)}$, $I_{(111m)}$, and $I_{(11\text{-}1m)}$ are the intensities of the peaks located at 2θ=30.2°, 31.2° and 28.2° in Fig. S4(a).

This ratio was almost constant for the films heat-treated at 600–1100°C, suggesting that the total volume fraction of the orthorhombic and tetragonal phases does not change much with the heat-treatment temperature.

Fig. 1(b) shows θ–2θ XRD patterns near {110} peaks located at 2θ = 21–27° integrated along the ψ direction of the data shown in Fig. S3. This measurement can distinguish the orthorhombic phase from the monoclinic phase because the {110} peak of the orthorhombic phase is located at 2θ = ~24.3°, but that of the monoclinic phase is located at 2θ = ~24°. No diffraction peaks corresponding to the tetragonal phase were observed. As-deposited and 600°C-heat-treated films showed only {110} peaks of the monoclinic phase, but films heat-treated above 900°C showed both {011} peaks of the monoclinic phase and {110} peaks of the orthorhombic phase. Fig. 2(b) shows the XRD intensity ratio, $I_{(110o)}/\{I_{(110o)}+ I_{(011m)}\}$, obtained from Fig. 1(b). Here, $I_{(110o)}$ and $I_{(011m)}$ are peak intensities of the peaks located at 2θ= 24.4° and 23.9° in Fig. S4(b), respectively. The intensity increased monotonically with increasing heat treatment temperature, suggesting that the volume fraction of the orthorhombic phase increased with increasing heat-treatment temperature.

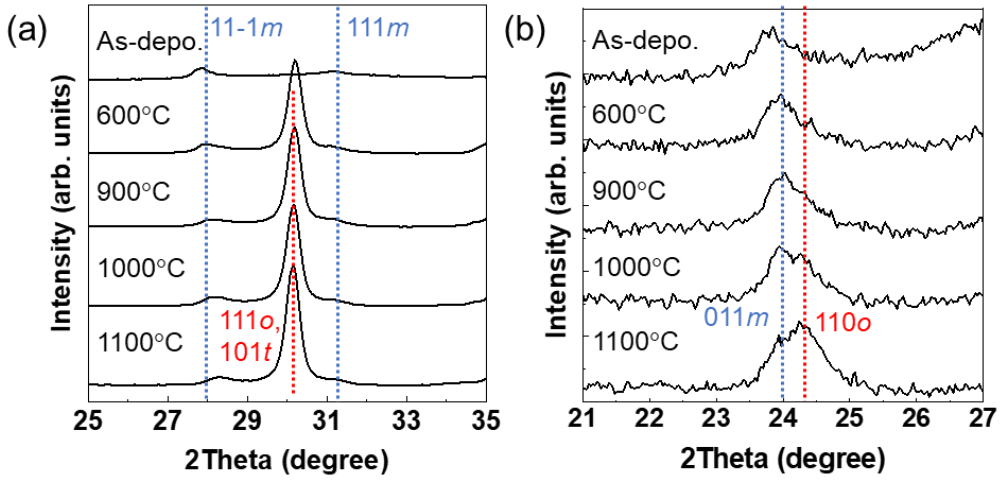

Fig. 1 θ–2θ XRD patterns at (a) 2θ = 25–35° integrated along the ψ axis of the data shown in Fig. S2, and (b) 2θ = 21–27° integrated along ψ axis of the data shown in Fig. S3.

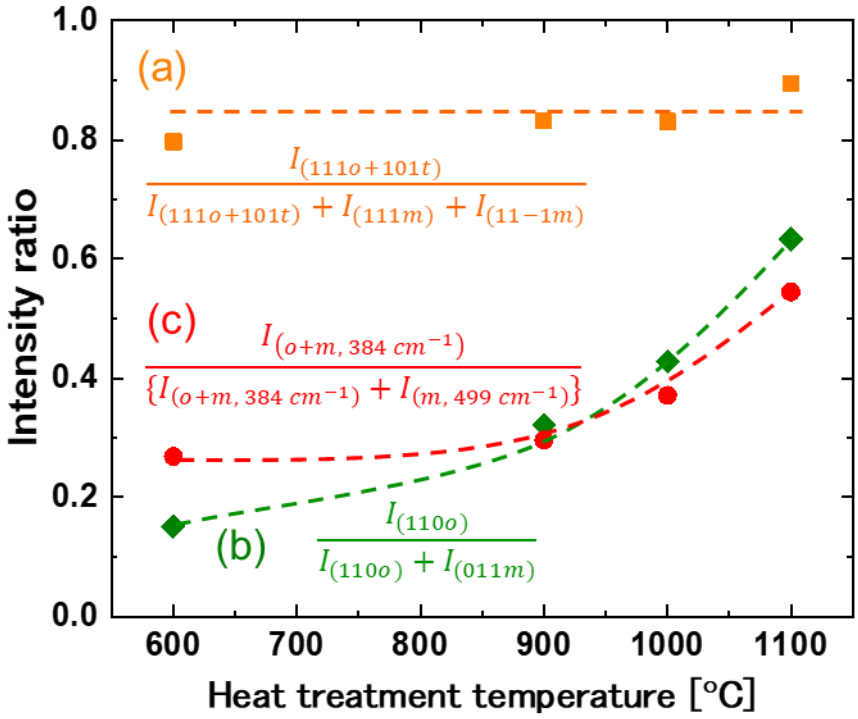

Fig. 2 (a) Heat-treatment temperature dependence of the $I_{(111o+101t)}/\{I_{(111o+101t)}+ I_{(111m)}+ I_{(11\text{-}1m)}\}$ ratio obtained from Fig. 1(a). Here, $I_{(111o+101t)}$, $I_{(111m)}$, and $I_{(11\text{-}1m)}$ are the peak intensities of the peaks located at 2θ = 30.2°, 31.2°, and 28.2° in Fig. S4(a), respectively. (b) Heat-treatment temperature dependence of the $I_{(110o)}/\{I_{(110o)}+ I_{(011m)}\}$ ratio obtained from Fig. 1(b). Here, $I_{(110o)}$ and $I_{(011m)}$ are the peak intensities of the peaks located at 2θ = 24.4° and 23.9° in Fig. S4(b), respectively. (c) Heat-treatment temperature dependence of the $I_{(o+m,\ 384\ cm^{-1})}/\{I_{(o+m,384\ cm^{-1})} + I_{(m,499\ cm^{-1})}\}$ ratio. Here, $I_{(o+m,384\ cm^{-1})}$ and

$I_{(m,499\,cm^{-1})}$ are the intensities of the Raman shifts located at 384 and 499 cm^{-1}, respectively.

Figures 3(a)–(d) show the *P–E* hysteresis loops of the 7%$YO_{1.5}$-93%HfO_2 films heat-treated at various temperatures. Ferroelectricity was not observed for the film heat-treated at 600°C, but clear hysteresis loops originating from the ferroelectricity were observed for the films heat-treated at 900–1100°C. Fig. 4 shows the remnant polarization (*P*r) obtained from the *P–E* curves shown in Fig. 3 as a function of the heat-treatment temperature. An almost constant *P*r value of approximately 16 μC/cm^2 was observed for the films heat-treated in the temperature range of 900 to 1100°C. This suggests that the volume fraction of the ferroelectric orthorhombic phase (*Pca*2_1) was almost constant because of the similar crystal orientations of the films (Figs. S1 and S2). As shown in Fig. 2, the XRD analysis revealed that the volume fraction of the orthorhombic phase monotonously increased with increasing heat-treatment temperature, although this analysis could not distinguish between the *Pca*2_1 and *Pbca* phases Two possible explanations for this exist. One explanation is that the volume fraction of the ferroelectric orthorhombic *Pca*2_1 phase was constant and only the volume fraction of the orthorhombic *Pbca* phase increased with temperature. The other explanation is that the field-induced phase transition from the tetragonal phase to the ferroelectric orthorhombic *Pca*2_1 phase occurred during *P–E* hysteresis measurements. To examine these possibilities, we carried out a Raman scattering study, which could distinguish between the two orthorhombic phases and other phases, as shown in Fig. S1. This measurement enabled the observation of phase changes by applying an electric field.

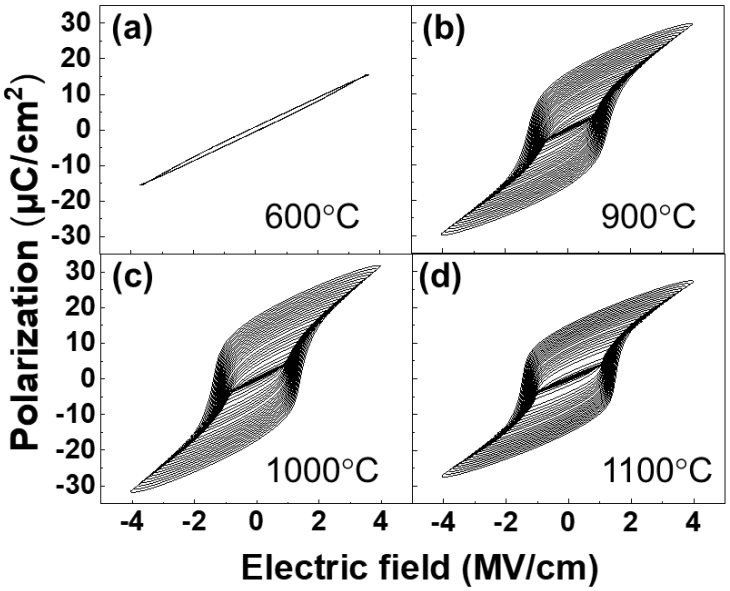

Fig. 3 *P–E* hysteresis loops measured at 10 kHz for 7%$YO_{1.5}$-93%HfO_2 films heat-treated at (a) 600, (b) 900, (c) 1000, and (d) 1100°C.

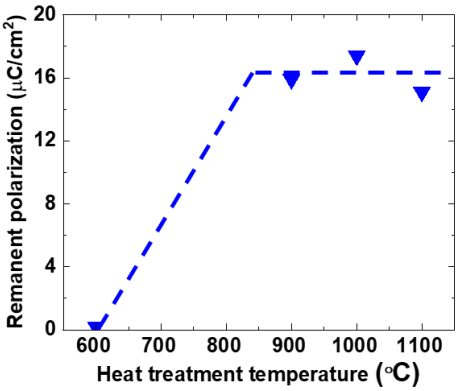

Fig. 4 Remanent polarization (*P*r) obtained from the *P–E* curves shown in Fig. 3 as a function of the heat-treatment temperature.

Fig. 5 shows the nonpolarized Raman spectra of the films heat-treated at various temperatures. This measurement was performed on the cross-section. We also show the

reported peak positions and intensities of Raman spectra for single crystalline orthorhombic *Pbca* (11%$YO_{1.5}$-89%HfO_2) and orthorhombic *Pca*2_1 (12%$YO_{1.5}$-88%HfO_2) phases by Fan *et al*. as a reference for orthorhombic phases.[11] Yashima *et al.* reported Raman spectra for arc-melted powders of Y-doped HfO_2 for monoclinic (HfO_2), orthorhombic γ_2 (7%$YO_{1.5}$-93%HfO_2), orthorhombic γ_1 (9%$YO_{1.5}$-91%HfO_2), and tetragonal (12%$YO_{1.5}$-88%HfO_2) phases.[18] They did not identify the space groups of the orthorhombic γ_1 and γ_2 phases, but these Raman spectra fit well with the *Pca*2_1 and *Pbca* phases shown by Fan *et al.*, respectively. These reports reveal that Y doping can help the metastable phase appear, even in bulk HfO_2. The experimental positions of the Raman spectra obtained by Yashima *et al*. are also shown in Fig. 5 as references for the monoclinic, orthorhombic, and tetragonal phases.

Specific peaks at 135, 149, and 499 cm^{-1} from the monoclinic phase and 115, 261, 308, 585, and 650 cm^{-1} from the tetragonal phase were observed for the films heat-treated at 600°C, suggesting that the films consisted of monoclinic and tetragonal phases. However, the intensities of the Raman peaks from the orthorhombic phases were quite weak owing to their weak XRD intensities, as shown in Fig. 1(a) and S4(b). Raman peaks at 156, 267, 319, 384, and 600 cm^{-1} from the ferroelectric non-centrosymmetric orthorhombic phase (*Pca*2_1) were detected for the films heat-treated above 900°C. Identification of the centrosymmetric orthorhombic phase (*Pbca*) from the most intense peak at 373 cm^{-1} was difficult because the peak overlapped with the peaks from the non-centrosymmetric orthorhombic phase at 384 cm^{-1} and the monoclinic phase at 383 and 399 cm^{-1}. However, since the specific peak at 423 cm^{-1} was not observed, the centrosymmetric orthorhombic phase (*Pbca*) was not included for all films. Therefore, the XRD peaks derived from the orthorhombic phase can be assumed to originate only from the non-centrosymmetric

*Pca*2$_1$ phase. The monoclinic, tetragonal, and orthorhombic *Pca*2$_1$ phases were included in the films heat-treated at 900 and 1000°C. Above 1100°C, the peak intensity at approximately 261 cm^{-1} from the orthorhombic *Pca*2$_1$ and tetragonal phases decreased dramatically. The intensities of other peaks from the orthorhombic *Pca*2$_1$ phase at 156, 319, 384, and 600 cm^{-1} increased, suggesting that the amount of the orthorhombic *Pca*2$_1$ phase increased. Considering that the most intense peak from the tetragonal phase was located at approximately 261 cm^{-1},[11,18,25] the decrease in the peak intensity at approximately 261 cm^{-1} was explained by a decreasing amount of tetragonal phase.

Although the remnant polarization value and Y concentration are quite different between the film and a single crystal in Y-doped HfO_2, the Raman positions of the *Pca*2$_1$ phase were not appreciably different. Fan *et al*. suggested that the difference in the polarization value was due to the strain from the substrate; however, the effect of strain on the Raman positions was not observed in our experiment. The investigation of the correlation between the polarization values and Raman positions for different strain states using thick Y-doped HfO_2 films is a topic for future work.

Fig. 2(c) also plots the intensity ratio of $I_{(o+m,\ 384\ cm^{-1})}/\{I_{(o+m,\ 384\ cm^{-1})} + I_{(m,\ 499\ cm^{-1})}\}$, where $I_{(o+m,\ 384\ cm^{-1})}$ and $I_{(m,\ 499\ cm^{-1})}$ are the intensities of the Raman shifts at 384 and 499 cm^{-1}, respectively. This intensity ratio increased with increasing heat-treatment temperature, suggesting that the orthorhombic *Pca*2$_1$ phase increased, consistent with the XRD results. The tetragonal phase was stable for all samples according to the Raman spectra, as shown in Fig. 5. The samples heat-treated at 900–1100°C show the same polarization values as shown in Fig. 4 despite different peak intensities of the *Pca*2$_1$ phase in both Fig. 2(b) and (c) obtained from XRD and Raman

scattering analysis, respectively.

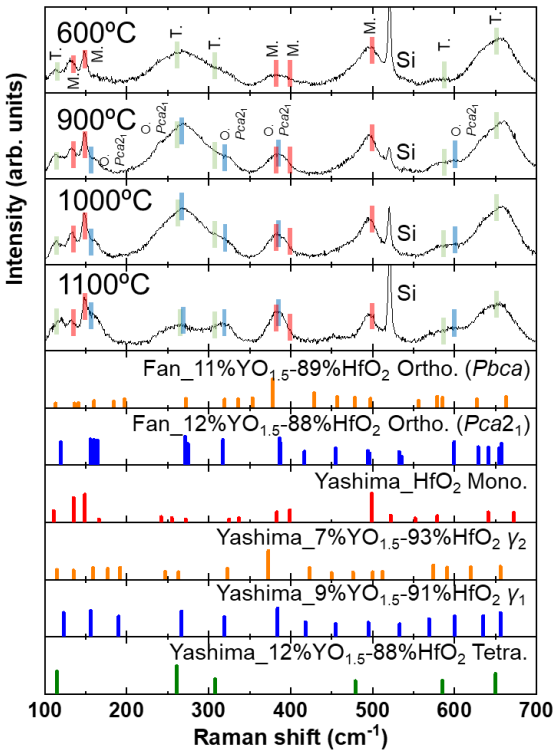

Fig. 5 Raman spectra of the films heat-treated at various temperatures measured from the cross-section of the film. Experimental normalized intensities and positions of Raman spectra for single crystals of orthorhombic *Pbca* (11%$YO_{1.5}$-89%HfO_2) and orthorhombic *Pca*2$_1$ (12%$YO_{1.5}$-88%HfO_2) phases by Fan *et al*. and arc-melted powder of monoclinic (HfO_2), γ_2 (7%$YO_{1.5}$-93%HfO_2), γ_1 (9%$YO_{1.5}$-91%HfO_2), and tetragonal phases by Yashima *et al*. are also shown. Here, the experimental result from the orthorhombic *Pca*2$_1$ (12%$YO_{1.5}$-88%HfO_2) phase of Fan *et al*. contains peaks from both out-of-plane and in-plane vibrations.[11,18]

As mentioned previously, a reasonable explanation for this discrepancy is the phase

transformation caused by the application of an electric field. To clarify this assumption, phase identification of the films after the application of an electric field is essential. For this analysis, Raman scattering is a more powerful tool than XRD because its spatial resolution is approximately 1 μm, even for a laboratory-scale machine, which is much smaller than that of XRD. However, observation of the top surface of the film on the top electrode area is required to observe the change in the Raman spectrum upon applying an electric field. Almost the same spectra were observed from the cross-section and the surface of the films heat-treated at 900 and 1100°C, as shown in Fig. S5.

The Raman spectrum before applying an electric field was detected from just outside of the Pt top electrode, while that after applying an electric field was obtained by the removal of the top electric field, as shown in Fig. 6(a) for the film heat-treated at 900°C. No obvious change in the Raman spectrum before and after the fabrication of the top electrode was observed. Fig. 6(b) and (c) shows the Raman spectra before and after applying an electric field to films heat-treated at 900 and 1100°C, respectively. Before applying the electric field, the peak intensity ratio $I_{(o+m,\ 384\ cm^{-1})}/\{I_{(o+m,\ 384\ cm^{-1})} + I_{(m,\ 499\ cm^{-1})}\}$ of the film heat-treated at 1100°C was larger than that heat-treated at 900°C. This indicates that the ferroelectric orthorhombic $Pca2_1$ phase increased with increasing heat-treatment temperature, as shown in the cross-section in Fig. 2. After applying an electric field, the ratio increased for the film heat-treated at 900°C but did not change much for that heat-treated at 1100 °C. This clearly shows the field-induced phase transition from the tetragonal phase to the ferroelectric orthorhombic $Pca2_1$ phase for the film heat-treated at 900°C. In addition, the peak at approximately 261 cm^{-1} weakened remarkably upon electric field application, which is the most intense peak in the tetragonal phase.

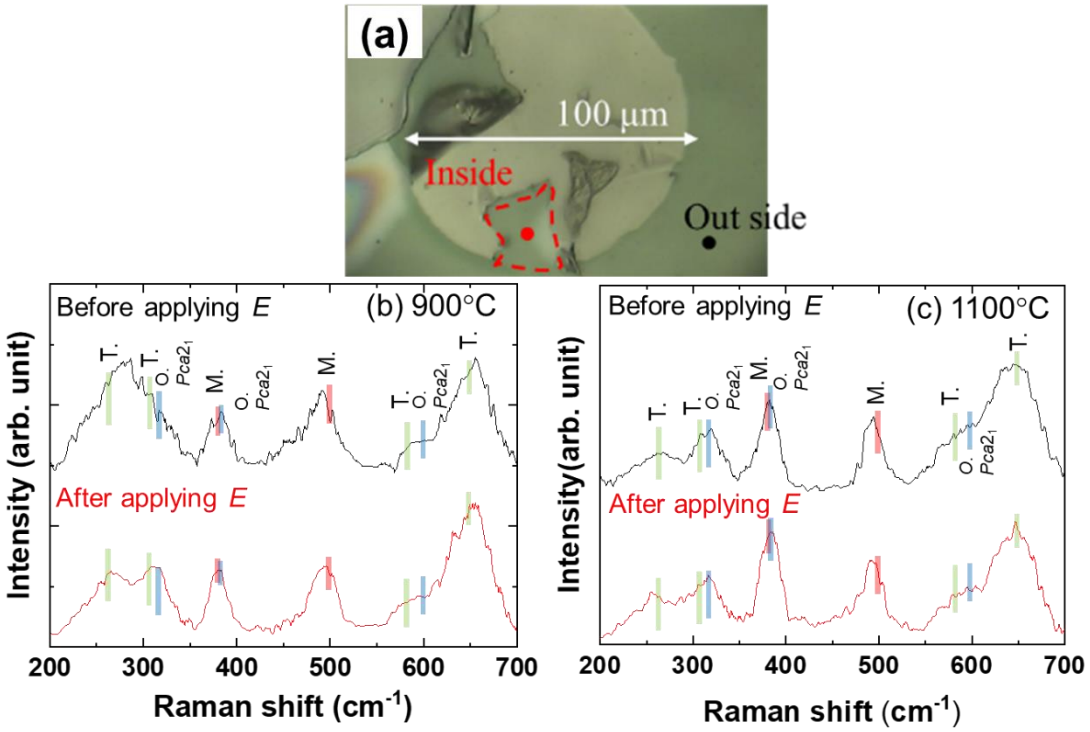

Fig. 6 (a) Optical microscopy image of the measurement point of the Raman spectrum before applying the electric field (just outside of the Pt top electrode) and after applying the electric field (after removal of the top electric field) for the film heat-treated at 900°C. The Raman spectrum before and after applying an electric field for films heat-treated at (b) 900 and (c) 1100°C deposited on Pt-coated Si substrates.

These results clearly show that Raman spectroscopy is a more powerful tool for phase identification than the widely used XRD technique because centrosymmetric (*Pbca*) and noncentrosymmetric orthorhombic phases ($Pca2_1$) can be identified. In addition, good spatial resolution on the order of several micrometers is also very useful for detecting field-induced phase changes, as demonstrated in this study, as well as for investigating the distribution of the ferroelectric phase on the surface. In addition, a strong signal was obtained from the cross-section of the thick Y-doped HfO_2 film.

Raman analysis of the thick film will be useful for future investigations of the relationship between the strain and crystalline phase in the film thickness direction.

4 Conclusions

In this study, we applied Raman spectroscopy to 850-nm-thick 7%$YO_{1.5}$-93%HfO_2 films. Raman spectroscopy of the cross-section can clearly distinguish between tetragonal, orthorhombic *Pbca*, and orthorhombic *Pca*2_1 phases, revealing the dependence of the constituent phases of heat-treated films on the heat-treatment temperature. A field-induced phase transition from the tetragonal to orthorhombic *Pca*2_1 phase was observed in the Raman spectra of the top surface. These results indicate that Raman spectroscopy is a powerful tool for identifying crystalline phases. Moreover, good Raman spectra were obtained from the cross-section as well as the surface of 850-nm-thick 7%$YO_{1.5}$-93%HfO_2 films. Therefore, high-resolution Raman spectroscopy in the film thickness direction has applications for research on the strain and phase distributions in thick films.

SUPPLEMENTARY MATERIAL

See the supplementary material for calculated Raman spectra and, XRD ψ–2θ scans near {111} and {110} peaks and comparison of Raman spectra measured from the cross-section and surface for the 7%$YO_{1.5}$-93%HfO_2 films heat-treated at various temperatures.

Acknowledgments

This research was partly supported by the Japan Society for the Promotion of Science (JSPS) KAKENHI grant numbers 21H01617, 19H00758, 22K18307, and 23K13364.

This work was partially supported by the MEXT Initiative to Establish Next-Generation Novel Integrated Circuit Centers (X-NICS)(JPJ011438) and the MEXT Program: Data Creation and Utilization Type Material Research and Development Project (JPMXP1122683430).

AUTHOR DECLARATIONS

Conflict of Interest

The authors have no conflict of interest to disclose.

Author Contributions

Takanori Mimura: Writing – original draft (lead). Yuma Takahashi: Writing – original draft (equal); Investigation (lead). Takahisa Shiraishi: Writing – review & editing (equal). Masanori Kodera: Writing – review & editing (equal); Investigation (equal). Reijiro Shimura: Investigation (equal). Keisuke Ishihama: Investigation (equal). Kazuki Okamoto: Writing – review & editing (equal); Investigation (equal). Hiroki Moriwake: Writing – review & editing (equal); Investigation (equal). Ayako Taguchi: Investigation (equal). Takao Shimizu: Writing – review & editing (equal). Yasuhiro Fujii: Writing – review & editing (equal). Akitoshi Koreeda: Writing – review & editing (equal); Investigation (equal). Hiroshi Funakubo: Supervision (equal); Writing – review & editing

(equal).

DATA AVAILABILITY

Data supporting the findings of this study are available from the corresponding authors upon request.

References

[1] T.S. Böscke, J. Müller, D. Bräuhaus, U. Schröder, and U. Böttger, "Ferroelectricity in hafnium oxide thin films," Appl. Phys. Lett. **99**(10), 102903 (2011).

[2] J. Müller, P. Polakowski, S. Mueller, and T. Mikolajick, "Ferroelectric hafnium oxide based materials and devices: Assessment of current status and future prospects," ECS. J. Solid State Sci. Technol. **4**(5), N30 (2015).

[3] R. Shimura, T. Mimura, A. Tateyama, T. Shiraishi, T. Shimizu, T. Yamada, Y. Tanaka, Y. Inoue, and H. Funakubo, "No-Heating Deposition of 1-μm-Thick Y-Doped HfO_2 Ferroelectric Films with Good Ferroelectric and Piezoelectric Properties by Radio Frequency Magnetron Sputtering Method," Phys. Status Solidi RRL **16**(10), 2100574 (2022).

[4] T. Schenk, N. Godard, A. Mahjoub, S. Girod, A. Matavz, V. Bobnar, E. Defay, and S. Glinsek, "Toward Thick Piezoelectric HfO_2-Based Films," Phys. Status Solidi RRL **14**(3), 1900626 (2020).

[5] T. Mimura, T. Shimizu, and H. Funakubo, "Ferroelectricity in $YO_{1.5}$-HfO_2 films around 1 μ m in thickness Ferroelectricity in $YO_{1.5}$-HfO_2 films around 1 μm in thickness," Appl. Phys. Lett. **115**, 032901 (2019).

[6] T. Shimizu, K. Katayama, T. Kiguchi, A. Akama, T.J. Konno, and H. Funakubo, "Growth

of epitaxial orthorhombic $YO_{1.5}$-substituted HfO_2 thin film," Appl. Phys. Lett. **107**(3), 032910 (2015).

[7] X. Sang, E.D. Grimley, T. Schenk, U. Schroeder, and J.M. LeBeau, "On the structural origins of ferroelectricity in HfO_2 thin films," Appl. Phys. Lett. **106**(16), 162905 (2015).

[8] T.D. Huan, V. Sharma, G.A. Rossetti, and R. Ramprasad, "Pathways towards ferroelectricity in hafnia," Phys. Rev. B **90**(6), 064111 (2014).

[9] T. Shiraishi, S. Choi, T. Kiguchi, T. Shimizu, H. Uchida, H. Funakubo, and T.J. Konno, "Fabrication of ferroelectric Fe doped HfO_2 epitaxial thin films by ion-beam sputtering method and their characterization," Jpn. J. Appl. Phys. **57**, 11UF02 (2018).

[10] Y. Cheng, Z. Gao, K.H. Ye, H.W. Park, Y. Zheng, Y. Zheng, J. Gao, M.H. Park, J.H. Choi, K.H. Xue, C.S. Hwang, and H. Lyu, "Reversible transition between the polar and antipolar phases and its implications for wake-up and fatigue in HfO_2-based ferroelectric thin film," Nat. Commun. **13**(1), 645 (2022).

[11] S. Fan, S. Singh, X. Xu, K. Park, Y. Qi, S.W. Cheong, D. Vanderbilt, K.M. Rabe, and J.L. Musfeldt, "Vibrational fingerprints of ferroelectric HfO_2," NPJ Quantum Mater. **7**(1), 32 (2022).

[12] A. Raeliarijaona, and R.E. Cohen, "First-principles calculations of Raman and infrared

spectroscopy for phase identification and strain calibration of hafnia," Appl. Phys. Lett. **120**(24), 242903 (2022).

[13] B. Zhou, H. Shi, X.D. Zhang, Q. Su, and Z.Y. Jiang, "The simulated vibrational spectra of HfO_2 polymorphs," J. Phys. D: Appl. Phys. **47**(11), 115502 (2014).

[14] A. Bartasyte, S. Margueron, J. Kreisel, P. Bourson, J. Santiso, C. Jimenez, A. Abrutis, F. Weiss, and M.D. Fontana, "Residual stress estimation in ferroelectric $PbTiO_3$ thin films by Raman spectroscopy," Phys. Rev. B **79**, 104104 (2009).

[15] S. Yokoyama, H. Morioka, Y.K. Kim, and H. Nakaki, "Crystal structure and microstructure of epitaxial $Pb(Zr,Ti)O_3$ films consisting of mixed phases with tetragonal and rhombohedral symmetries grown on $(100)_c SrRuO_3$//$(100)SrTiO_3$ substrate by metalorganic chemical vapor deposition," J. Mater. Res. **22**(6), 1551 (2007).

[16] M. Nakajima, H. Nakaki, Y. Ehara, T. Yamada, K. Nishida, T. Yamamoto, M. Osada, and H. Funakubo, "In situ Raman spectroscopy for characterization of the domain contributions to electrical and piezoelectric responses in $Pb(Zr,Ti)O_3$ films," Appl. Phys. Lett. **97**, 181907 (2010).

[17] S. Starschich, T. Schenk, U. Schroeder, and U. Boettger, "Ferroelectric and piezoelectric properties of $Hf_{1-x}Zr_xO_2$ and pure ZrO_2 films," Appl. Phys. Lett. **110**(18),

182905 (2017).

[18] M. Yashima, H. Takahashi, K. Ohtake, T. Hirose, M. Kakihana, H. Arashi, Y. Ikuma, Y. Suzuki, and M. Yoshimura, "Formation of metastable forms by quenching of the HfO_2-$RO_{1.5}$ melts (R = Gd, Y and Yb)," J. Phys. Chem. Solids **57**(3), 289 (1996).

[19] X. Xu, F.T. Huang, Y. Qi, S. Singh, K.M. Rabe, D. Obeysekera, J. Yang, M.W. Chu, and S.W. Cheong, "Kinetically stabilized ferroelectricity in bulk single-crystalline HfO_2:Y," Nat. Mater. **20**(6), 826 (2021).

[20] M. Materano, P. Reinig, A. Kersch, M. Popov, M. Deluca, T. Mikolajick, U. Boettger, and U. Schroeder, "Raman Spectroscopy as a Key Method to Distinguish the Ferroelectric Orthorhombic Phase in Thin ZrO_2-Based Films," Phys. Status Solidi RRL **16**(4), 2100589 (2022).

[21] U. Schroeder, R. Sachdeva, P.D. Lomenzo, B. Xu, M. Materano, T. Mikolajick, and A. Kersch, "Using Raman spectroscopy and x-ray diffraction for phase determination in ferroelectric mixed $Hf_{1-x}Zr_xO_2$-based layers," J. Appl. Phys. **132**(21), 214104 (2022).

[22] B. Xu, P.D. Lomenzo, A. Kersch, T. Mikolajick, and U. Schroeder, "Influence of Si-Doping on 45 nm Thick Ferroelectric ZrO_2 Films," ACS Appl. Electron. Mater. **4**(7), 3648 (2022).

[23] C.Q. Luo, C.Y. Kang, Y.L. Song, W.P. Wang, and W.F. Zhang, "Large remanent

polarization in Ta-doped HfO_2 thin films by reactive sputtering," Appl. Phys. Lett. **119**(4), 042902 (2021).

[24] T. Shiraishi, K. Katayama, T. Yokouchi, T. Shimizu, T. Oikawa, O. Sakata, H. Uchida, Y. Imai, T. Kiguchi, T.J. Konno, and H. Funakubo, "Effect of the film thickness on the crystal structure and ferroelectric properties of $(Hf_{0.5}Zr_{0.5})O_2$ thin films deposited on various substrates," Mater. Sci. Semicond. Process **70**, 239 (2017).

[25] Y.K. Voronko, A.A. Sobol, and V.E. Shukshin, "Monoclinic-tetragonal phase transition in zirconium and hafnium dioxides: A high-temperature Raman scattering investigation," Phys. Solid State **49**(10), 1963 (2007).

Fig.1

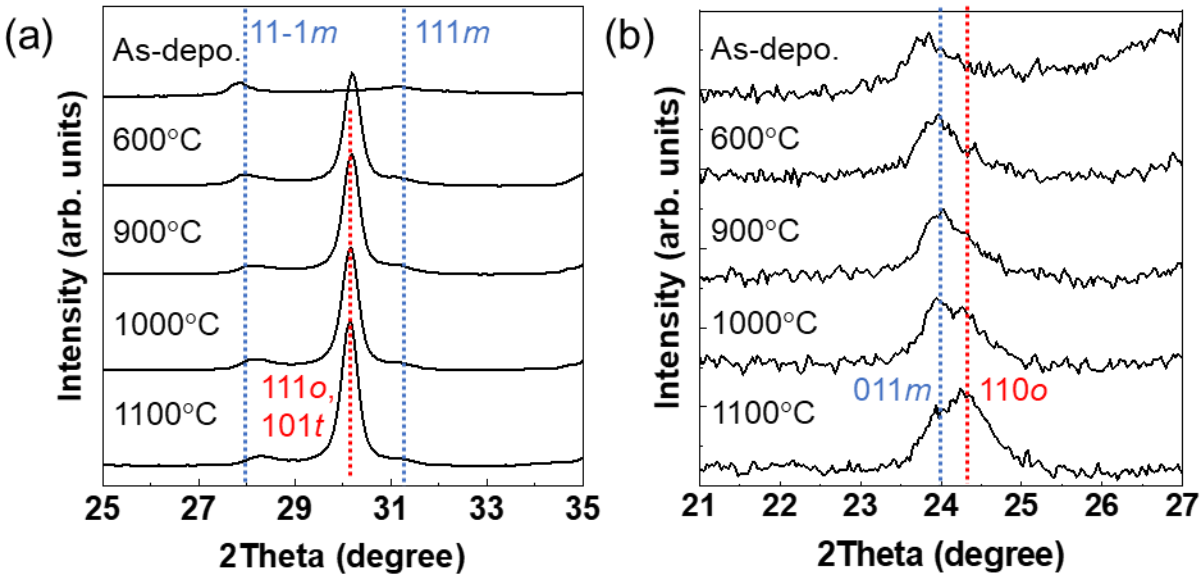
(a)
As-depo.
600°C
900°C
1000°C
1100°C
11-1m
111m
111o,
101t
Intensity (arb. units)
25
27
29
31
33
35
2Theta (degree)
(b)
As-depo.
600°C
900°C
1000°C
1100°C
011m
110o
Intensity (arb. units)
21
22
23
24
25
26
27
2Theta (degree)

Fig.2

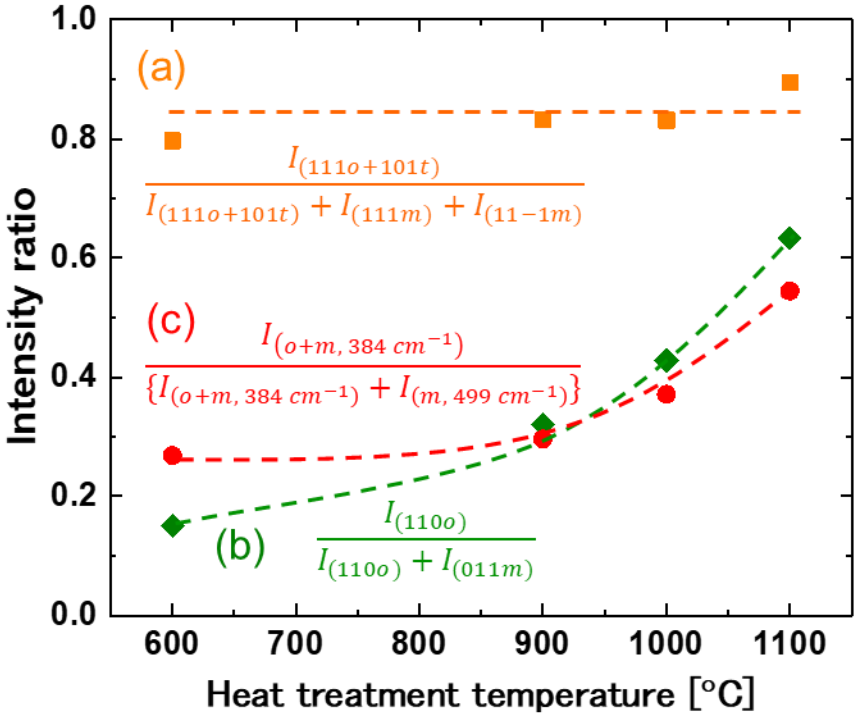
1.0
0.8
0.6
0.4
0.2
0.0
Intensity ratio
600
700
800
900
1000
1100
Heat treatment temperature [°C]
(a)
$\frac{I_{(111o+101t)}}{I_{(111o+101t)} + I_{(111m)} + I_{(11-1m)}}$
(c)
$\frac{I_{(o+m,\,384\ cm^{-1})}}{\{I_{(o+m,\,384\ cm^{-1})} + I_{(m,\,499\ cm^{-1})}\}}$
(b)
$\frac{I_{(110o)}}{I_{(110o)} + I_{(011m)}}$

Fig.3

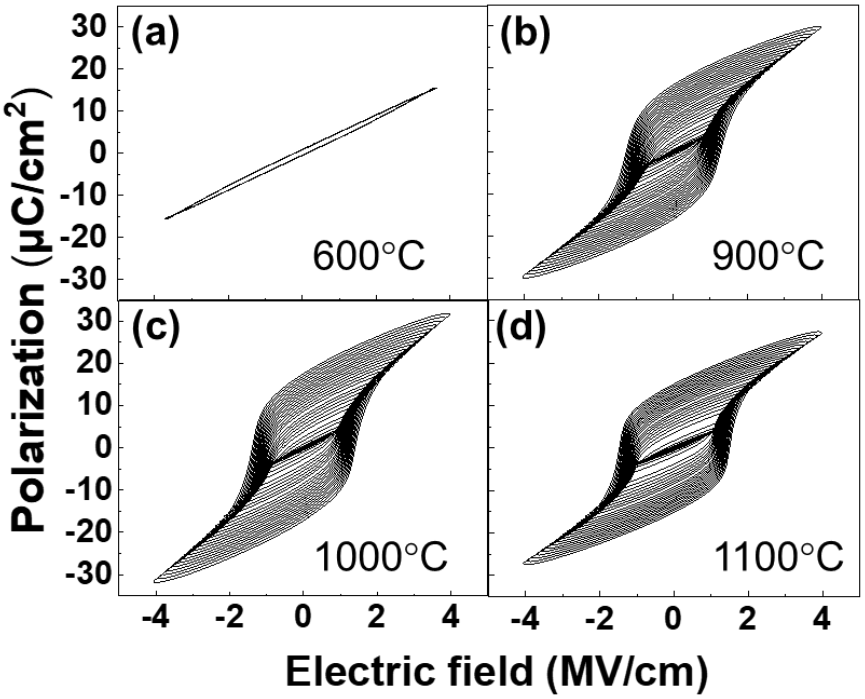
(a)
600°C
(b)
900°C
(c)
1000°C
(d)
1100°C
Polarization (μC/cm²)
Electric field (MV/cm)
30
20
10
0
-10
-20
-30
-4
-2
0
2
4

Fig.4

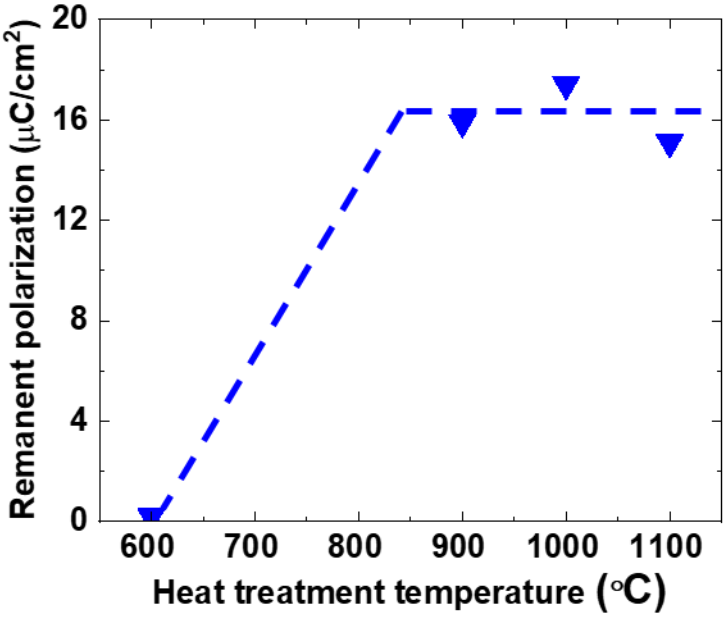
Remanent polarization (μC/cm²)
20
16
12
8
4
0
600
700
800
900
1000
1100
Heat treatment temperature (°C)

Fig.5

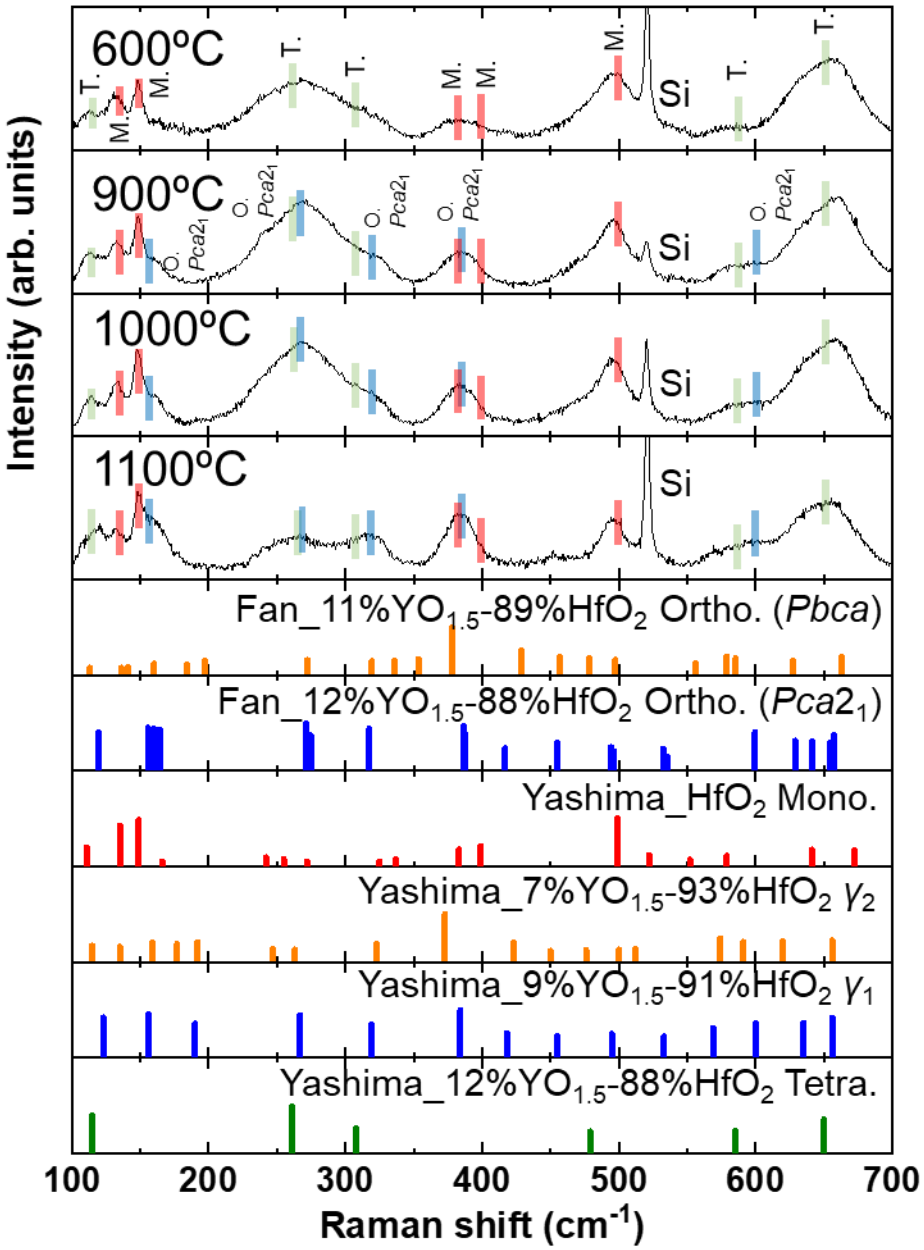
600ºC
900ºC
1000ºC
1100ºC
T.
M.
O.
Pca2₁
Si
Intensity (arb. units)
Fan_11%YO1.5-89%HfO2 Ortho. (Pbca)
Fan_12%YO1.5-88%HfO2 Ortho. (Pca2₁)
Yashima_HfO2 Mono.
Yashima_7%YO1.5-93%HfO2 γ2
Yashima_9%YO1.5-91%HfO2 γ1
Yashima_12%YO1.5-88%HfO2 Tetra.
100
200
300
400
500
600
700
Raman shift (cm-1)

Fig.6

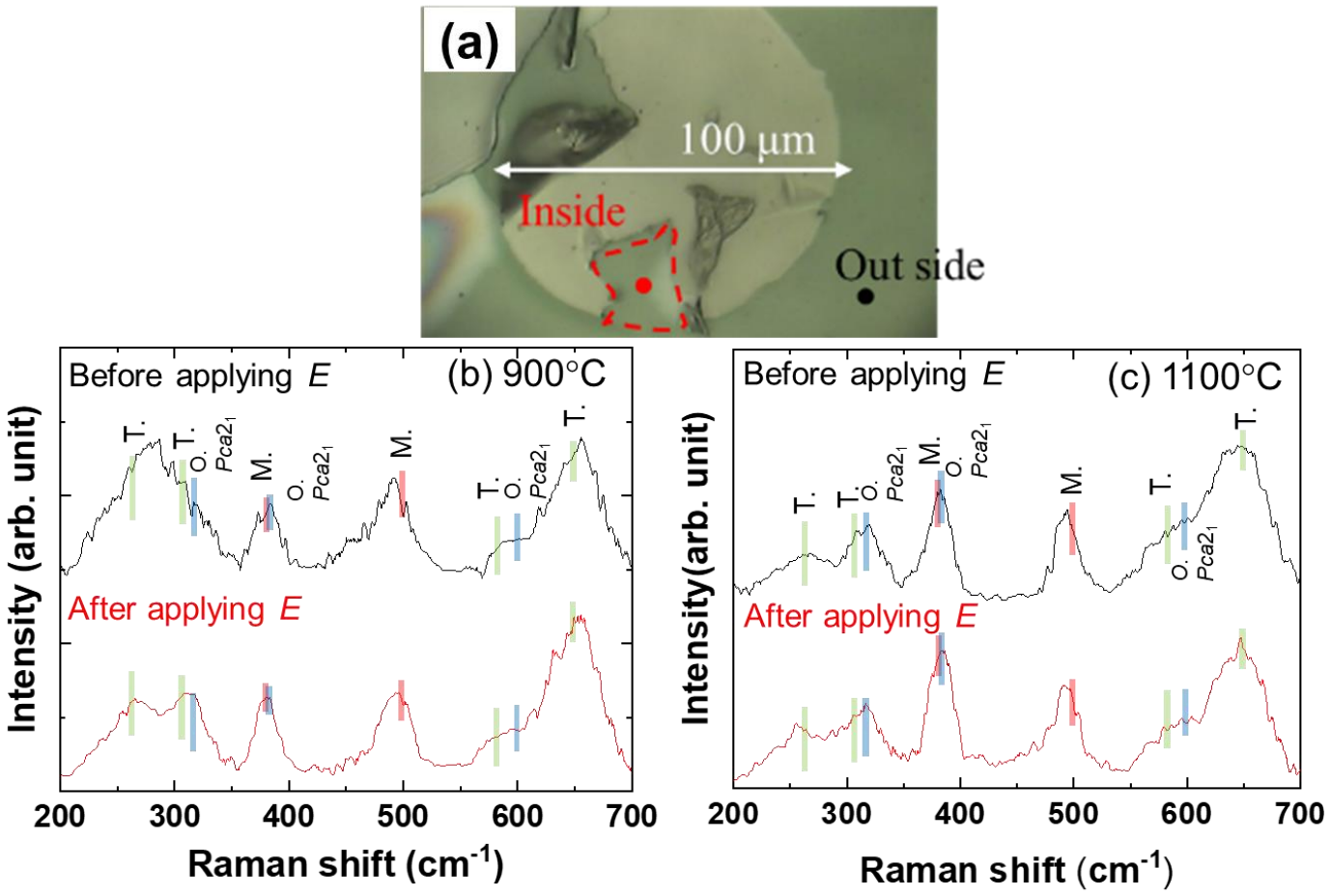
(a)
100 μm
Inside
Out side
Before applying E
(b) 900°C
After applying E
Intensity (arb. unit)
T.
O. Pca2₁
M.
Raman shift (cm⁻¹)
200
300
400
500
600
700
Before applying E
(c) 1100°C
After applying E
Intensity(arb. unit)
Raman shift (cm⁻¹)